

PCCP

Accepted Manuscript



This is an *Accepted Manuscript*, which has been through the Royal Society of Chemistry peer review process and has been accepted for publication.

Accepted Manuscripts are published online shortly after acceptance, before technical editing, formatting and proof reading. Using this free service, authors can make their results available to the community, in citable form, before we publish the edited article. We will replace this *Accepted Manuscript* with the edited and formatted *Advance Article* as soon as it is available.

You can find more information about *Accepted Manuscripts* in the [Information for Authors](#).

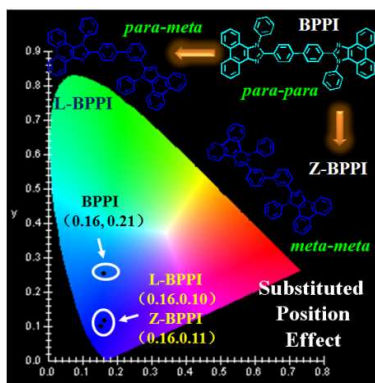
Please note that technical editing may introduce minor changes to the text and/or graphics, which may alter content. The journal's standard [Terms & Conditions](#) and the [Ethical guidelines](#) still apply. In no event shall the Royal Society of Chemistry be held responsible for any errors or omissions in this *Accepted Manuscript* or any consequences arising from the use of any information it contains.

Graphical Abstract

for *Physical Chemistry Chemical Physics*

**Dimeric Phenanthroimidazole for Blue Electroluminescent Materials:
The Effect of Substituted Position Attaching to Biphenyl Center**

Zhiming Wang^{a*}, Ying Feng^a, Hui Li^a, Zhao Gao^b, Xiaojuan Zhang^a, Ping Lu^b,
Ping Chen^{c*}, Yuguang Ma^b, Shiyong Liu^c



The more valuable deep emission is realized by tuning substituted position on biphenyl from *para*-coupling to *meta*-one.

Cite this: DOI: 10.1039/c0xx00000x

www.rsc.org/xxxxxx

ARTICLE TYPE

Dimeric Phenanthroimidazole for Blue Electroluminescent Materials: The Effect of Substituted Position Attaching to Biphenyl Center

Zhiming Wang^{*a}, Ying Feng^a, Hui Li^a, Zhao Gao^b, Xiaojuan Zhang^a, Ping Lu^b, Ping Chen^{*c}, Yuguang Ma^b, Shiyong Liu^c

Received (in XXX, XXX) Xth XXXXXXXXX 20XX, Accepted Xth XXXXXXXXX 20XX
DOI: 10.1039/b000000x

As two isomers of 4,4'-bis(1-phenyl-phenanthro[9,10-d]imidazol-2-yl)biphenyl (**BPPI**), **L-BPPI** and **Z-BPPI** were prepared by tuning substituted position on biphenyl from *para*- to *meta*-coupling. Because of the conjugated degree change at C2-position in phenanthroimidazole block, the fluorescent color of **L-BPPI** (433 nm) and **Z-BPPI** (402 nm) showed obvious blue-shift compared with **BPPI** (468 nm) in the films. Meanwhile, their non-doped devices exhibited more valuable and stable deep-blue emissions with CIE coordinate of (0.16, 0.10) and (0.16, 0.11), respectively. Furthermore, some valuable structure-properties information was analyzed by density functional theory (DFT) calculations, photophysical and electrochemical characterization.

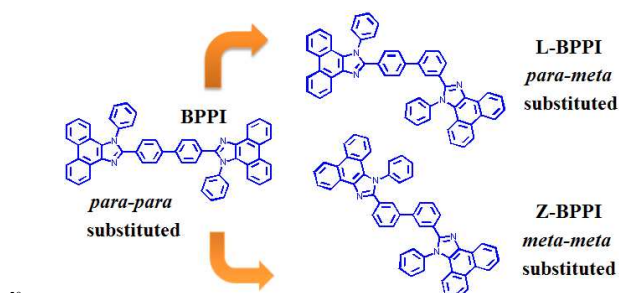
1. Introduction

Organic light-emitting devices (**OLEDs**) have attracted considerable attentions due to their potential applications in full color flat panel displays during the past decades.^[1] Up to now, with the rapid improvement in performances of **OLEDs**, large amounts of efficient fluorescence and phosphorescence emitters have already emerged. However, there are still some vital problems to be addressed, such as the lack of highly efficient and stable deep-blue emitting materials with good color purity, economical operation towards the practical industrial application, and so on.^[2]

Recently, the wholly aryl-substituted phenanthroimidazole (WAPI), as an efficient deep-blue emitter block, has attracted tremendous attentions due to its simple synthesis process, excellent thermal properties, high fluorescence quantum yields (reference) and potential "bipolar" properties.^[3-10] As the non-doped blue emitters, the external quantum efficiency of their derivatives in devices could extend 5 % with CIE_y < 0.15 by Ma and Tong.^[5,7] And as the doped blue fluorescent emitters or hosts, highly efficient white or phosphorescent **OLEDs** are also realized by Ge and Wang et al.^[8-10]

Previous theoretical calculation and experimental results reveal the substituted group at C2-position in WAPI played an important role in their fluorescent properties, for the substituted group at C2-position greatly determines the molecular conjugated degree of the WAPI derivatives. Tong et al. employed a strongly conjugated unit thiophene ring (TPA-TPI) to replace the benzene ring (TPA-BPI) at this position, and a red-shift of 30 nm was observed in both solution and solid state from TPA-BPI to TPA-TPI.^[7a] Park and co-workers replaced the phenol with naphthalen-2-ol at the C2-position of HPNIC, the fluorescent color was shifted from 450 nm to 580 nm in solution (CHCl₃).^[11]

Lin group introduced an ion chelated bipyridyl group into the C2-phenyl group and extended this oligomer to become an efficient fluorescent sensor of Fe³⁺.^[12]



Scheme 1 The structures of **BPPI**, **L-BPPI** and **Z-BPPI**

Compound 4,4'-bis(1-phenyl-phenanthro[9,10-d]imidazol-2-yl) biphenyl (**BPPI**) was reported in our previous paper as an excellent blue-emitting material with high electroluminescence performance in simple non-doped device.^[4a] As a class dimeric phenanthroimidazole (**DPI**), **BPPI** exhibited the higher thermal stability and fluorescent efficiency, as well as more balanced charge injection property, than the single phenanthroimidazole **PPI** and trimeric phenanthroimidazole **TPPI**. But it is a pity that its emission was red-shifted from 421 nm in solution to 468 nm in film, and thus the CIE coordinates of the double-layered device was obtained at (0.16, 0.21), which deviated from the blue light area according to the standards ($x + y < 0.30$) specified by the National Television Standards Committee (**NTSC**).^[13] The data of full-width at half-maximum (**FWHM**) of **BPPI** showed that the red-shift in film not only came from the aggregation in the solid state, but also originated from the change of the excited state structure, for the planarization effect of biphenyl center would cause the π -electron delocalization in wide system.^[3a, 4e] In order to weaken the change of conjugated degree at C2-position

to realize the deep blue emission in the solid state, the *para*-coupling one of biphenyl at C2-position was replaced by the alternative *meta*-coupling way, which was employed because of its feeble conjugation ability.

Herein, 3,4'-bis(1-phenyl-phenanthro[9,10-d]-imidazol-2-yl) biphenyl (**L-BPPI**) and 3,3'-bis(1-phenyl-phenanthro[9,10-d]-imidazol-2-yl)biphenyl (**Z-BPPI**) were designed and prepared as shown in Scheme 1. Both derivatives are isomers of **BPPI**. By tuning the substituted position on biphenyl center, the fluorescence of **L-BPPI** (433 nm) and **Z-BPPI** (402 nm) were obviously blue-shifted than **BPPI** (468 nm) in the films, and the non-doped devices based on **L-BPPI** and **Z-BPPI** as emitters exhibited the stable deep blue emissions with CIE coordinates of (0.16, 0.10) and (0.16, 0.11) respectively. The newcomers maintained higher thermal stability, proper carrier barriers and balanced charge injection property like **BPPI**, and possessed certain suppressed aggregation ability. As a successful example, the structure-properties relationship of **L-BPPI** or **Z-BPPI** reveals not only more information about the C2 substituted group, but also the new designing idea for other WAPI derivatives.

2. Materials and Measurement

All the reagents and solvents used for the synthesis were purchased from Aldrich or Acros companies and used as received. All reactions were performed under a dry nitrogen atmosphere.

The ^1H NMR spectra were recorded on AVANCZ 500 spectrometers at 298K by utilizing deuterated dimethyl sulphoxide (**DMSO**) as solvent and tetramethylsilane (**TMS**) as standard. The compounds were characterized by Flash EA 1112, CHNS-O elemental analysis instrument. The MALDI-TOF-MS mass spectra were recorded using an AXIMA-CFRTM plus instrument. UV-vis absorption spectra were recorded on UV-3100 spectrophotometer. Fluorescence measurements were carried out with RF-5301PC. The fluorescence quantum yield in solution was measured using 0.5 M H_2SO_4 solution of quinine as reference (0.54), and the solid state quantum yield on the quartz plate was measured by an integrating sphere apparatus using **Alq₃** as reference (0.22). The differential scanning calorimeter (DSC) analysis was determined using a NETZSCH (DSC-204) instrument at 10 °C/min under nitrogen flushing. Cyclic voltammetry (CV) were performed with a BAS 100W Bioanalytical Systems, using a glass carbon disk ($\Phi = 3$ mm) as working electrode, platinum wire as auxiliary electrode with porous ceramic wick, Ag/Ag^+ as reference electrode, standardized for the redox couple ferricinium/ferrocene. All solutions were purged with nitrogen stream for 10 min before measurement. The procedure was performed at room temperature and nitrogen atmosphere was maintained over the solution during measurements.

3. Device Fabrication

The EL devices were fabricated by vacuum deposition of the materials at 10^{-6} Torr onto ITO glass with a sheet resistance of 25 Ω square⁻¹. All of the organic layers were deposited at a rate of 1.0 \AA s⁻¹. The cathode was deposited with Mg and Ag at a

deposition rate of 2 \AA s⁻¹. The electroluminescence (EL) spectra and CIE coordination of these devices were measured by a PR650 spectra scan spectrometer. The luminance-current and density-voltage characteristics were recorded simultaneously with the measurement of the EL spectra by combining the spectrometer with a Keithley model 2400 programmable voltage-current source. All measurements were carried out at room temperature under ambient conditions.

4. Synthesis and characterization

4.1 Synthesis

As shown in experimental section, **BPPI**, **L-BPPI** and **Z-BPPI** were synthesized by a one-pot reaction.^[3-12] The mixture of aniline, phenanthrenequinone, ammonium acetate and the corresponding biphenyl dicarboxaldehyde were refluxed in acetate acid for 2 hours, and then poured into the stirring methanol solution. After filtering, the crude product was purified by chromatography and the yield was above 70% as our previous report. The biphenyldicarboxaldehyde was prepared by the Suzuki-coupling reaction with the yield over 80% by using commercial bromobenzaldehyde or formylphenylboronic acid (as shown in Supporting Information).^[14]

4.2 NMR characterization

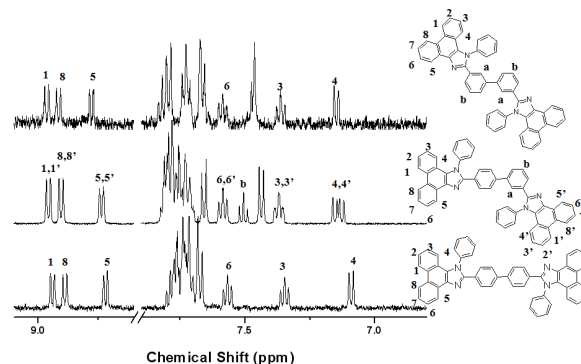


Fig.1 ^1H NMR spectra of **BPPI**, **L-BPPI** and **Z-BPPI** in the aromatic range.

Fig. 1 shows the ^1H NMR spectra of **BPPI**, **L-BPPI** and **Z-BPPI** in the aromatic range. Compared with the symmetric structure of **BPPI** and **Z-BPPI**, the fine split of **L-BPPI** spectrum shows more detailed structure information. The four doublets around 8.95, 8.90, 8.75 and 7.10 ppm are considered to derive from the characteristic protons resonance in phenanthroimidazole block from the hydrogen at 1, 4, 5, 8-positions of the phenanthrene unit.^[4] Compared with the 1, 5, 8-positions located at phenanthroimidazole peripheral space, the chemical environments of the protons change little by the structure tuning in the three **DPI** since they exhibit the similar chemical shift at the lower filed. While, the one doublet at 7.10 ppm in **BPPI** and **Z-BPPI** (marked as 4) is split into two neighboring couples doublets in **L-BPPI** (marked as 4 and 4'), and the fine difference is owing to the similar protons in different chemical environments. This split is also consistent with our guess about the response from 4-position at phenanthrene unit.^[15]

The strongest evidence for the target compounds **L-BPPI** and **Z-BPPI** is the singlet at the a-position, but this proton resonance overlaps with the peaks from other aromatic hydrogen.

However, a new triplet with 1/34 integral area appears at 7.51 ppm in **L-BPPI** spectrum, which is corresponding to the proton resonance at the b-position. Unfortunately, this couple of triplet (2/34) is not observed clearly in **Z-BPPI**, for this response is also

5 disturbed from other hydrogen in the aromatic range. The detailed information of protons resonance is shown in the inserted illustration of Fig. 1, and all the peaks observed in the ^1H NMR spectra correspond well to the respective structures. This accurate confirmation is also beneficial to the structure

4.3 Thermal properties

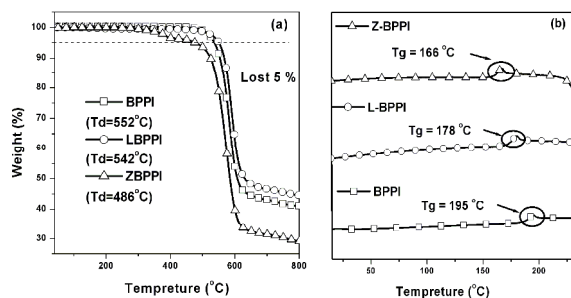


Fig.3 The TGA (a) and DSC (b) curves of **BPPI**, **L-BPPI** and **Z-BPPI**

15 The thermal properties of **BPPI**, **L-BPPI**, **Z-BPPI** are investigated by thermal gravimetric analyses (TGA) and differential scanning calorimetry (DSC) under a nitrogen atmosphere (Fig. 3). The three compounds show similar decomposition progress, the temperatures at a 5% weight loss

20 (T_d) are 552 °C for **BPPI**, 542 °C for **L-BPPI** and 486 °C for **Z-BPPI**, respectively. The obvious decrease may originate from the reduced stacking density in block. Take **Z-BPPI** as an example, it owns a symmetrical structure as **BPPI**, but two different optimized conformations (Z-shape and C-shape in Fig. 4) in

25 space, which would induce the condensed molecular packing more hardly, and the congestion degree is even lower than **L-BPPI**.^[16]

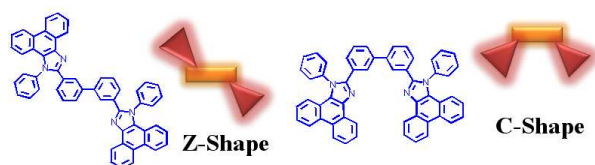


Fig.4 Two conformation of **Z-BPPI** in space

The speculation is tested in subsequent measurement of the glass transition temperature (T_g), and the value continues to slow down from 195 °C for **BPPI**, to 178 °C for **L-BPPI**, and to 166 °C for **Z-BPPI**, which is due to the loose packing forms giving

35 molecules enough internal space to tune its conformation with lower energy barriers.^[16] Nevertheless, the three **DPI** derivatives exhibit higher T_g values (>150 °C) than common organic compounds, implicating that they could form morphologically stable amorphous films upon thermal evaporation. All of these

40 properties are highly important for their applications in **OLEDs**.

4.3 Theoretical Calculations

To get an insight into the molecular and electronic structures

of the three oligomers, the Gaussian 03 program is used to perform quantum chemical calculations. As shown in Fig. 5, in

45 all three **DPI**, the phenyl moieties attached to N1 are nearly perpendicular to the phenanthro[9,10-d]imidazol planes with the angle of about 80 °. As our known, the conjugated degree at this large angle is very limited, and the wave function shows little overlap with the PI moiety, not participating in the formation of

50 frontier molecular orbital. The two dihedral angles (the one between the phenyl group attaching C2 and the phenanthroimidazole, and the other one between the two benzene units in the biphenyl center) are around 30°, indicating that a large enough π -electron overlap was very easy to form by this

55 biphenyl conjugated-bridge between the two PI moieties at C2-position. The distribution and delocalization rang of π -electron would be influenced from the different coupling positions to the bridge.^[17] Additionally, the large planar structure of phenanthroimidazole at every oligomer terminal is observed,

60 which is tend to form overlapping π - π system between two neighbouring molecules to cause the molecular aggregation or microcrystal, consequently leading to a large PL red-shift. This initiative π - π stacking phenomenon would benefit the charge transport in **OLEDs**.

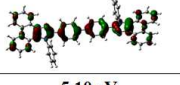
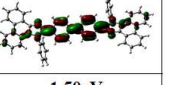
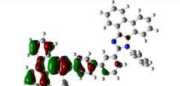
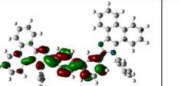
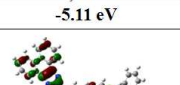
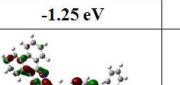
	HOMO	LUMO	GAP
BPPI	 -5.10 eV	 -1.50 eV	3.60 eV
L-BPPI	 -5.11 eV	 -1.25 eV	3.86 eV
Z-BPPI	 -5.17 eV	 -1.06 eV	4.12 eV

Fig.5 The electronic structures (the frontier molecular orbitals) of **BPPI**, **L-BPPI** and **Z-BPPI** (at the B3LYP/6-311+G-d level graphs)

The electron-density distribution of the HOMO for the

70 oligomers is localized predominantly on the electron-rich phenanthro[9,10-d]imidazole (PI) planes, and the HOMO values from theoretical calculation in the three WAPI derivatives are very close each other. The distribution of LUMO shows the same trend to HOMO, mostly distributing on the biphenyl center with a

75 small fraction on PI moiety, but their values are increased from -1.50 to -1.06 eV because of gradually limited π -electron delocalization rang from *para-para* to *meta-meta* form. As our expected, their corresponding band-gaps are also increased, along with the decrease of the conjugated ability at C2-position.^[18]

80 Additionally, some degree of space-charge-separation ability is found in **L-BPPI** and **Z-BPPI**, which would be benefit for the injection of carriers from electrode. The calculated values of the energy levels from DFT have the same tend, and the results are confirmed by the further photo and electrochemical experiments.

4.4 Photophysical properties

As can be seen in the absorption spectra in THF solutions (10^{-5} M), there is a sharp absorption peak at 260 nm for the three compounds (Fig. 6a), and which is attributed to typical electronic transition from the phenyl group attached to **N1** in **DPI** derived compounds.^[4] Compared with the *para-para* coupling form in **BPPI**, the *para-meta* and *meta-meta* ones using C2-biphenyl-bridge exhibit gradually the limited π -electron delocalization range as shown in Fig. 5, and the π - π^* electronic transition shifts from 314 nm for **Z-BPPI**, to 329 nm for **L-BPPI**, and to 369 nm for **BPPI**. In fine spectrum of **L-BPPI**, there are two obvious shoulder absorption peaks at 289 and 361 nm, which are matched well with the fine splits of **BPPI** (289 nm) and **Z-BPPI** (361 nm). This detail implies the **L-BPPI** had the similar electronic transition to the **BPPI** and **Z-BPPI** as illustrated. Although these fine structures are not observed in their solid state, the blue-shift of π - π^* absorption transition in **L-BPPI** and **Z-BPPI** are also observed.

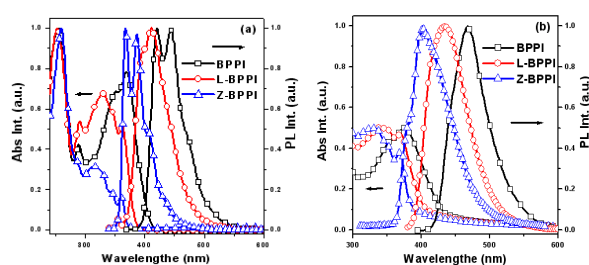


Fig. 6 Normalized absorption and emission spectra of **BPPI**, **L-BPPI** and **Z-BPPI** in THF (10^{-5} M) (a) and in films (b)

More valuable results could be obtained from the photoluminescence spectra. The emission peak at 421 nm in **BPPI** shifts to 411 nm in **L-BPPI** and 368 nm in **Z-BPPI** in THF solutions (Fig. 6a). This trend also maintains in the solid state as described in Fig. 6b, the sky-blue emission of **BPPI** (emission peak 468 nm) is changed to deep-blue emissions in **L-BPPI** and **Z-BPPI** with peaks at 434 and 402 nm, respectively. The blue shift of emission spectra in **L-BPPI** and **Z-BPPI** mainly originates from the effective conjugated degree change at C2-position. As shown in Fig. 5, the π -electron in each PI unit

becomes harder to move towards the other one from **BPPI** to **Z-BPPI** due to the coupling way adjustment from *para*-form to *meta*-one. This gradually limited π -electron delocalization usually causes the increased band-gaps and the blue-shift emission as above, which are also consistent with the spectra above and the increase of band-gap values in **L-BPPI** and **Z-BPPI**, as DFT described. Additionally, the gradual decrease of the fluorescence quantum yields is observed in solution and solids from **BPPI** to **Z-BPPI**, which indicates that this *meta*-coupling way may cause the loss of the fluorescent transition ratio.

As a combiner of *para*-form and *meta*-one, **L-BPPI** exhibits higher efficiencies and more valuable blue emission in solution and films as list in Table-1. Compared to the larger red-shift in **BPPI** (47 nm) and **Z-BPPI** (34 nm) from solution to film, this difference in **L-BPPI** is only 23 nm. The obvious asymmetric spatial structure is an important reason for such a slight value, and would reduce the order stacking in block and weaken the aggregation effects in certain degree.

5.5 CV measurement

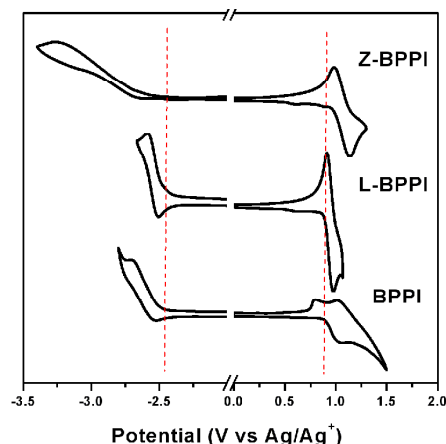


Fig. 7 The CV curves of **BPPI**, **L-BPPI** and **Z-BPPI**.

Table 1 The thermal, photophysical and electrochemistry data of **BPPI**, **L-BPPI** and **Z-BPPI**

	T_g ($^{\circ}$ C)	T_d^a ($^{\circ}$ C)	PL ^b / Φ_n^c λ_{max} (nm) (soln)	PL ^d / Φ_n^e λ_{max} (nm) (film)	E_{onset}^{ox} (V)	E_{onset}^{red} (V)	HOMO (eV)	LUMO (eV)	E _{gap} (eV)
BPPI	195	535	421/0.92	468/0.85	0.89	-2.43	-5.47	-2.29	3.18
L-BPPI	178	542	411/0.68	434/0.57	0.89	-2.35	-5.48	-2.33	3.15
Z-BPPI	166	486	368/0.55	402/0.35	0.98	-2.61	-5.48	-2.18	3.30

a. The temperature for 5% weight loss of the oligomers; b. The maximum peak in solution; c. The fluorescence quantum yield in solution compared to 0.5 M H_2SO_4 solution of quinine as a reference (0.54); d. The thickness of the film are 50 nm; e. the solid state quantum yield was measured by an integrating sphere apparatus using **Alq₃** as reference (0.22); e. The energy levels were calculated using the energy level of the ferrocene (Fc) reference (4.8 eV) and calibrated using $E_{1/2}(Fc/Fc^+)$.

The CV measurement in solution is conducted in CH_2Cl_2 and DMF mixture (1:1) with 0.1 M tetra-n-butylammonium-hexafluorophosphate ($n-Bu_4NPF_6$) as electrolyte at room temperature. **HOMO** and **LUMO** levels are estimated using the

energy level of the ferrocene (Fc) reference (4.8 eV) and calibrated with $E_{1/2}(Fc/Fc^+)$ in every measurement^[19]. Their cyclic voltammograms are shown in Fig. 7 and the respective electrochemical data are summarized in Table 1. **L-BPPI** and **Z-**

BPPI exhibits the similar re-dox progress as **BPPI** in the positive potential region. This couple of oxidation/re-reduction peak with the onset oxidation potential ($E_{\text{onset}}^{\text{ox}}$) is at about 0.9 V vs Ag wire, and the **HOMO** level is calculated to be -5.48 eV after calibrating. Such similar values testify that the oxidation progress would happen in their common PI unit.

In the negative potential region, the same onset reduction potential ($E_{\text{on-set}}^{\text{red}}$) about -2.40 V vs Ag wire is observed in **BPPI** and **L-BPPI**, and the **LUMO** levels is calculated to be -2.29 eV for **BPPI** and -2.33 eV for **L-BPPI** after calibrating. This indicates that there was a similar reduction in their structures, which might originate from *para*-substituted phenanthro[9,10-d]-imidazol-2-yl biphenyl structure as marked in Fig.5. Thus, this point is further confirmed by the data from the **LUMO** level of -2.18 eV for **Z-BPPI**, the only *meta*-substituted coupling performs the higher energy level than the *para*-substituted ones with higher conjugated degree.

All these details are consistent with the results of molecular simulation that **HOMO** was localized at PI unit and **LUMO** was localized at biphenyl unit with different form, and the band gap is widen from **BPPI** to **Z-BPPI** as DFT estimated. Additionally, the **L-BPPI** shows obvious “bipolar” character with the quasi-reversible re-dox process in CV measurement, and might be a potential compound as high performance blue emitter.^[20]

4.6 Single-carrier device

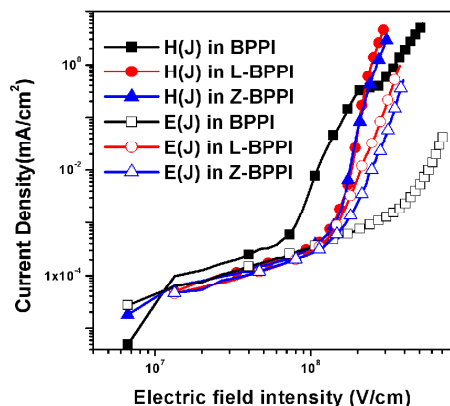


Fig.8 The current density–electric field intensity curves of the single-carriers devices based on **BPPI**, **L-BPPI** and **Z-BPPI**

In order to better understand the effect of the structural change on the energy level and the carrier injection/transport ability, the hole-only and the electron-only devices of **L-BPPI**, **Z-BPPI** and **BPPI** were fabricated, respectively^[21]. The configuration of hole-only device is ITO/**BPPI** (or **L-BPPI** or **Z-BPPI**, 90 nm)/Au (100 nm) and the electron-only device has the configuration of ITO/TPBi (10 nm)/**BPPI** (or **L-BPPI** or **Z-BPPI**, 90 nm)/LiF (1 nm)/Al (100 nm). In electron-only device, the 10 nm TPBi is inserted as a hole-blocking layer to ensure the pure electron current in device.

It can be seen from Fig. 8 that the hole-current density (J) in **L-BPPI** or **Z-BPPI** is lower than **BPPI** though they have the very close HOMO values. This decrease might originate from the irregular spatial structure of **L-BPPI** and **Z-BPPI**. But the electron current is higher, which might be caused by the coupling way of biphenyl group. When the electric field intensity increased, the closer electron current and hole current density is observed in **L-BPPI** and **Z-BPPI**, which reveals that the more balanced charge injection-transport was performed in their devices.

4.7 EL properties

The non-doped devices with typical multi-layer structures of ITO/m-M-MoO_x(30 nm)/NPB (20 nm)/ Emitter (x nm)/ TPymbi (50-x nm)/Mg:Ag (10:1 by weight, 100 nm) are fabricated to investigate the potential applications of the compounds in the blue OLEDs, in which MoO_x is employed as the carriers modified layers, and the 3TPymbi (tris[3-(3-pyridyl)mesityl]borane) is inserted to tune electron injection barriers by the thickness.^[22]

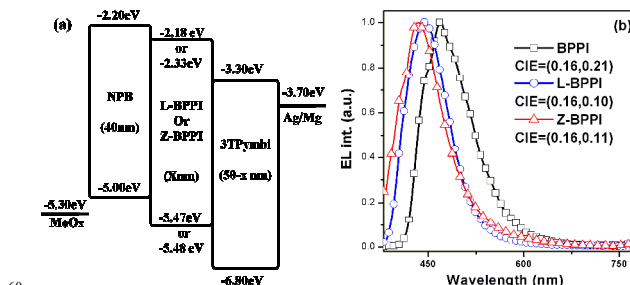


Fig.9 (a) the EL devices structure; (b) the EL spectra of the devices in 9V

Table 2 The devices performance of **BPPI**, **L-BPPI** and **Z-BPPI**.

Device Structure		Voltage ^a [V]	L_{Max} [cd/m ²]	LE_{Max} [cd/A]	CIE [x, y]		Voltage ^a [V]	L_{Max} [cd/m ²]	LE_{Max} [cd/A]	CIE [x, y]
A (x=50nm)	L-BPPI	8.5	70	0.01	0.16,0.11	Z-BPPI	6.5	105	0.07	0.17,0.12
B (x=40nm)	L-BPPI	6.5	295	0.13	0.16,0.11	Z-BPPI	5.0	502	0.34	0.16,0.12
C (x=30nm)	L-BPPI	5.0	420	0.40	0.16,0.10	Z-BPPI	4.5	267	0.45	0.16,0.11
D (x=20nm)	L-BPPI	4.5	391	0.68	0.16,0.10	Z-BPPI	5.0	100	0.31	0.16,0.11

65 a. The turn-on voltage ($L > 1 \text{ cd/m}^2$)

All these devices exhibit the deep blue emissions with a maximum peak at ~440 nm and corresponding CIE coordinate of (0.16, 0.11), indicating an obvious blue-shift compared to 468 nm

70 with CIE coordinates of (0.16, 0.21) for **BPPI** in our previous report. The values satisfy the blue standards ($x + y < 0.30$) specified by the NTSC, as we expected.^[4, 11] These results suggest that it was a simple and efficient strategy to realize the

fluorescent color tuning by slight alteration at C2-position in WAPI-based material.

Although all the devices show low luminance, a basic trend is identified based on the data provided in Table 2. In the same measurement, with an increase in the thickness of 3iPYMB, the luminous efficiency (LE) of the **L-BPPI**-based device increases, and the turn-on voltage decreases from 8.5 to 4.5 V. These observations imply that more balanced carriers' injection/transportation is realized in Device D with a 3iPYMB thickness of 30 nm. The ideal thickness of the electron-modified layer in **Z-BPPI** is observed in device C. These similar results confirm that both **L-BPPI** and **Z-BPPI** show comparative carriers injection/transportation ability as the above mentioned single-carrier device. However, **L-BPPI** exhibits a greater LE with better color purity, involving better thermal stability and higher fluorescence efficiency, indicating that it is a superior candidate for a potential non-doped blue-light-emitting material.

5. Conclusion

In summary, we have developed two newborn **DPI** derivatives by tuning substituted position on biphenyl center from *para*- to *meta*-coupling one. As isomers of **BPPI**, **L-BPPI** and **Z-BPPI** show more valuable deep-blue fluorescence in the films and EL devices. Further comparison results of DFT, photo and electro characterization reveal much more important structure-property relationship information, such as the changes of color emission and efficiency. These observations from a simple adjustment at C2 position convince us that it is a strategy of chemical modification to enhance materials' properties.

Acknowledgements:

This work is financially supported by National Science Foundation of China (Grant No. 51203091, 60907013, 61377026), Liaoning Province Doctor Startup Fund (Grant No. 20131084) and Open Project of State Key Laboratory of Supramolecular Structure and Materials (sklssm201423).

Notes and references

^a School of Petrochemical Engineering, Shenyang University of Technology, 30 Guanghua Street, Liaoyang, 111003, P. R. China Fax: +86 419 5319409; Tel: +86 419 5319409; E-mail: wangzhm1983@163.com

^b State Key Laboratory of Supramolecular Structure and Materials, Jilin University, 2699 Qianjin Avenue, Changchun 130012, P.R.China.

^c State Key Laboratory on Integrated Optoelectronics, College of Electronic Science and Engineering, Jilin University, 2699 Qianjin Avenue, Changchun 130012, P.R.China.

† Electronic Supplementary Information (ESI) available: [details of any supplementary information available should be included here]. See DOI: 10.1039/b000000x/

‡ Experimental: Preparation of **BPPI** and **L(or Z)-BPPI**

The synthetic route of **BPPI** is reported in our privouse report, and the **L(or Z)-BPPI** shows the similar progress as the above one. A mixture of phenanthrene-9,10-dione (2.08 g, 10 mmol), 4-aminobenzonitrile (3.57 g, 30 mmol), ammonium acetate (3.85 g, 50 mmol) and 3,4'(or 3,3')-biphenyldicarboxaldehyde (1.01g, 4.8 mmol) were refluxed in acetate

acid for 2 hours, then poured into a methanol solution with stirring. After filtering, the crude product was purified by column chromatography, and the whit powder was gained.

L-BPPI : (2.84g, Yield:73.6%) ¹H NMR (500 MHz, DMSO, ppm): 8.97 (d, 2H), 8.91 (d, 2H), 8.74 (d, 2H), 7.82–7.70 (m, 17H), 7.67 (d, 2H), 7.58 (t, 2H), 7.51 (t, 1H), 7.45(d, 2H), 7.37 (t, 2H), 7.16-7.12(m, 2H). MALDI-TOF (*m/z*): [M⁺] calcd. C₅₄H₃₄N₄, 738.28; found, 739.9. Anal Calc. for C₅₄H₃₄N₄: C, 87.78; H, 4.64; N, 7.58. Found: C, 87.67; H, 4.61; N, 7.55.

Z-BPPI : (2.76g, Yield:75.4%) ¹H NMR (500 MHz, DMSO, ppm): 8.97 (d, 2H), 8.92 (d, 2H), 8.78 (d, 2H), 7.83-7.79 (m, 6H), 7.75-7.71 (m, 6H), 7.67-7.64 (m, 6H), 7.61 (t, 2H), 7.48 (m, 4H), 7.38 (t, 2H), 7.15 (d, 2H). MALDI-TOF (*m/z*): [M⁺] calcd. C₅₄H₃₄N₄, 738.28; found, 741.0. Anal Calc. for C₅₄H₃₄N₄: C, 87.78; H, 4.64; N, 7.58. Found: C, 87.76; H, 4.64; N, 7.57.

- (a) C.W. Tang and S. A. VanSlyke, *Appl. Phys. Lett.*, 1987, **51**, 93; (b) J. H. Burroughes, D. D. C. Bradley, A. R. Brown, R. N. Marks, K. Mackay, R. H. Friend, P. L. Born and A. B. Holmes, *Nature*, 1990, **347**, 539.
- M. R. Zhu, C. L. Yang, *Chem. Soc. Rev.*, 2013, **42**, 4963.
- (a) C. J. Kuo, T. Y. Li, C. C. Lien, C. H. Liu, F. I. Wu, M. J. Huang, *J. Mater. Chem.*, 2009, **19**, 1865-1871; (b) C. H. Cheng, C. H. Liu, F. I. Wu, 2010, *U.S. Patent No. 20100253208*.
- (a) Z. M. Wang, P. Lu, S. M. Chen, Z. Gao, F. Z. Shen, W. S. Zhang, Y. X. Xu, H. S. Kwok and Ma Y. G. *J. Mater. Chem.*, 2011, **21**, 5451; (b) Z. M. Wang, Z. Gao, S. F. Xue, Y. L. Liu, W. S. Zhang, C. Gu, F. Z. Shen, P. Lu and Y. G. Ma. *Polym. Bull.*, 2012, **69**, 273; (c) Z. M. Wang, X. H. Song, Z. Gao, D. W. Yu, X. J. Zhang, P. Lu, F. Z. Shen, Y. G. Ma, *RSC Adv.*, 2012, **2**, 9635.
- (a) W. J. Li, D. D. Liu, F. Z. Shen, D. G. Ma, Z. M. Wang, T. Feng, Y. X. Xu, B. Yang, Y. G. Ma. *Adv. Funct. Mater.*, 2012, **22**, 2797-2803; (b) Z. Gao, Y. L. Liu, Z. M. Wang, F. Z. Shen, H. Liu, G. N. Sun, L. Yao, Y. Lv, P. Lu, Y. G. Ma, *Chem. Eur. J.*, 2013, **19**, 2602.
- (a) Y. Yuan, D. Li, X. Q. Zhang, X. J. Zhao, Y. Liu, J. Y. Zhang, Y. Wang, *New J. Chem.*, 2011, **35**, 1534; (b) K. Wang, F. C. Zhao, C. G. Wang, S. Y. Chen, D. Chen, H. Y. Zhang, Y. Liu, D. G. Ma, Y. Wang, *Adv. Funct. Mater.*, 2013, **23**, 2672.
- (a) Y. Zhang, S. L. Lai, Q. X. Tong, M. F. Lo, T. W. Ng, M. Y. Chan, Z. C. Wen, J. He, K. S. Jeff, X. L. Tang, W. M. Liu, C. C. Ko, P. F. Wang, C. S. Lee, *Chem. Mater.*, 2012, **24**, 61; (b) Y. Zhang, S. L. Lai, Q. X. Tong, M. Y. Chan, T. W. Ng, Z. C. Wen, G. Q. Zhang, S. T. Lee, H. L. Kwong and C. S. Lee *J. Mater. Chem.*, 2011, **21**, 8206.
- H. Huang, Y. X. Wang, S. Q. Zhuang, X. Yang, L. Wang, C. L. Yang, *J. Phys. Chem. C*, 2012, **116**, 19458.
- S. Q. Zhuang, R. G. Shangguan, J. J. Jin, G. L. Tu, L. Wang, J. S. Chen, D. G. Ma, X. Ji Zhu, *Org. Electro.*, 2012, **13**, 3050.
- (a) J. L. Wang, W. Y. Lin, W. L. Li, *Biomaterials.*, 2013, **34**, 7429; (b) X. Y. Zhang, J. Lin, X. H. Ouyang, Y. Liu, X. Y. Liu, Z. Y. Ge, *J. Photochem. Photobiol., A*, 2013, **268**, 37.
- (a) Park S., Kwon J. E., Kim S. H., Seo J., Chung K., Park S. Y., Jang D. J., Medina B. M., Gierschner J., Park S. Y., *J. Am. Chem. Soc.* 2009, **131**, 14043–14049; (b) Park S., Kwon O., Lee Y., Jang D. J., Park S. Y., *J. Phys. Chem. A*, 2007, **111**, 9649–9653.
- Lin W. Y., Long L. L., Yuan L., Cao Z. M., Feng J. B., *Analytica Chimica Acta*, 2009, **634**, 262.
- (a) S. Tang, M. R. Liu, P. Lu, H. Xia, M. Li, Z. Q. Xie, F. Z. Shen, C. Gu, H. Wang, B. Yang, Y. G. Ma, *Adv. Funct. Mater.*, 2007, **17**, 2869; (b) C. Poriel, J. J. Liang, J. Rault-Berthelot, F. Barriere, N. Cocherel, A. M. Z. Slawin, D. Horhant, M. Virboul, G. Alcaraz, N. Audebrand, L. Vignau, N. Huby, G. Wantz, L. Hirsch, *Chem. Eur. J.*, 2007, **13**, 10055; (c) M. Santra, H. Moon, M. H. Park, T.-W. Lee, Y. K. Kim, K. H. Ahn, *Chem. Eur. J.*, 2012, **18**, 9886.
- T. Ishiyama, M. Murata, N. Miyauro, *J. Org. Chem.*, **1995**, 60, 7508.
- Botana E., Nättinen K., Prados P., Rissanen K., Mendoza J., *Org. Lett.*, 2004, **6**, 1091
- Jiang Z. Q., Liu Z. Y., Yang C.L., Zhong C., Qin J. G., Yu G., Liu Y. Q., *Adv. Funct. Mater.*, 2009, **19**, 1
- Zhang S. T., Li W. J., Yao L., Pan Y. Y., Shen F. Z., Xiao R., Yang B. Ma Y. G., *Chem. Commun.*, 2013, **49**, 11302

-
18. Lu P., Zhang H. Q., Li M., Zheng Y., Ma Y. G., Chen X. F., Tamai N., *Polym. Int.*, 2008, **57**, 987.
19. Z. M. Wang, X. H. Song, L. L. Ma, Y. Feng, C. Gu, X. J. Zhang, P. Lu, Y. G. Ma, *New J. Chem.*, 2013, **37**, 2440
- 5 20. Yao L., Xue S. F., Wang Q., Dong W. Y., Yang W., Wu H. B., Zhang M., Yang B., Ma Y. G., *Chem. Eur. J.*, 2012, **18**, 2707.
21. A. Chaskar, H. F. Chen, K. T. Wong, *Adv. Mater.*, 2011, **23**, 3876.
22. (a) Chen P., Xie W. F., Li J., Guan T., Duan Y., Zhao Y., Liu S. Y., Ma C. S., *Appl. Phys. Lett.*, 2007, **91**, 023505; (b) Chen P., Xue Q. Xie W. F., Duan Y., Xie G. H., Zhao Y., Hou J. Y., Liu S. Y., Zhang L. Y., Li B., *Appl. Phys. Lett.*, 2008 **93**, 153508; (c) Chen P., Xue Q. Xie W. F., Duan Y., Xie G. H., Zhao Y., Hou J. Y., Liu S. Y., Zhang L. Y., Li B., *Appl. Phys. Lett.*, 2009 **95**, 123307.
- 10